Photovoltaic Devices Made from Plasma-Doped Two-Dimensional Layered Semiconductors

Samuel Arthur
Physics, Colby College

NNIN REU Site: Lurie Nanofabrication Facility, University of Michigan, Ann Arbor, MI
NNIN REU Principal Investigator: Assistant Professor Xiaogan Liang, Mechanical Engineering, University of Michigan
NNIN REU Mentor: Sungjin Wi, Department of Mechanical Engineering, University of Michigan
Contact: sdarthur@colby.edu, sjwi@umich.edu, xiaoganl@umich.edu

Abstract:

Two-dimensional (2D) layered transition metal dichalcogenides (LTMDs, especially WSe_2 and MoS_2) exhibit a high absorption of visible light. For example, a LTMD monolayer (~ 0.5 nm) can absorb as much sunlight as 50-nm-thick silicon (Si) films [1]. Therefore, they are suitable for making next-generation ultrathin, flexible photovoltaic (PV) devices. However, society lacks the device physics knowledge and skills for generating built-in potentials in such emerging layered materials, which are required to separate photo-generated electron-hole pairs and create photocurrents. This REU project sought to leverage the plasma-doping method and vertically stacked LTMD heterostructures developed by Prof. Liang's group to create and optimize PV devices made from multilayer WSe_2 films with plasma-doping-induced p-n junctions. To achieve this goal, we fabricated PV devices with a vertically stacked indium tin oxide (ITO)/WSe_2/Au structure, using 2D layer printing, photolithography, thin-film deposition/lift-off, and plasma etching/doping. Our results provide critical information for identifying the band diagram of WSe_2 PV devices as well as optimizing their PV performance. This work provides scientific insights of the unique optoelectronic properties of 2D LTMDs at the backbone of emerging atomically layered PV devices.

Introduction:

LTMDs have a potential for making ultrathin photovoltaic (PV) devices that have great flexibility, high light-absorbing efficiency, long lifetime and low manufacturing cost. Molybdenum disulfide (MoS_2), a semiconducting LTMD, has recently been observed by Liang's group as a photovoltaic material. Tungsten diselenide (WSe_2) is another LTMD that has a similar layered structure to MoS_2 but has been anticipated to have the higher light absorption coefficients over a broader wavelength range in comparison with MoS_2. However, the PV response characteristics of WSe_2-based devices still remain poorly studied. Especially, the research society needs new scientific and technical schemes to form reliable p-n junctions (or built-in potentials) in such layered semiconductors, which is expected to be very different from the junction formation schemes for conventional semiconductors.

The goal of our project was to fabricate and characterize WSe_2-based photovoltaic cells with plasma-formed p-n junctions. In a PV process, the incident photons excite electrons from the valence band to the conduction band, creating electron-hole (e-h) pairs. The built-in field of the p-n junction can separate e-h pairs and result in a splitting of quasi-Fermi levels of electrons and holes as well as a photocurrent in the external circuit.

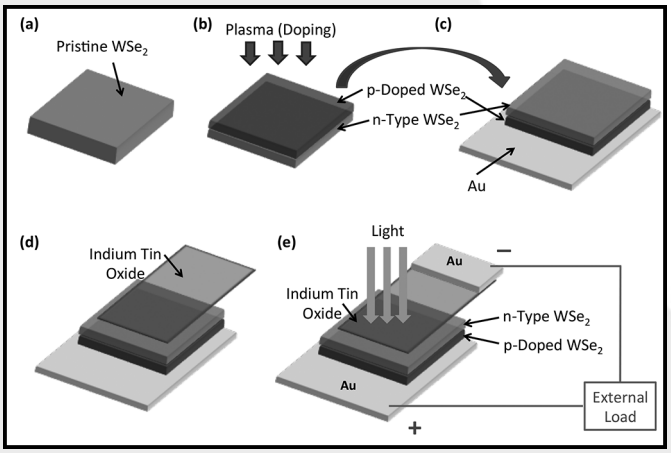

Figure 1: Schematic of the fabrication process.

Experimental Procedure:

The schematic diagram of the device fabrication process is illustrated in Figure 1. Adhesive tape squares were used to exfoliate pristine WSe_2 flakes from a bulk WSe_2 ingot (1a). The exfoliated $WSe2_2$ flakes were then thinned by repeatedly applying them to multiple adhesive tape squares. The tape squares containing the pristine WSe_2 flakes were treated with fluoroform (CHF_3) by reactive-ion etching (1b). These flakes were subsequently bonded onto wafers containing gold

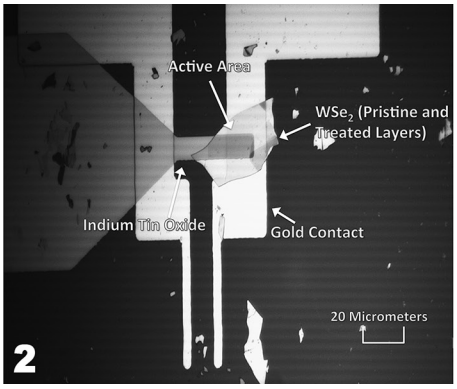

Figure 2: Completed photovoltaic cell diagram.

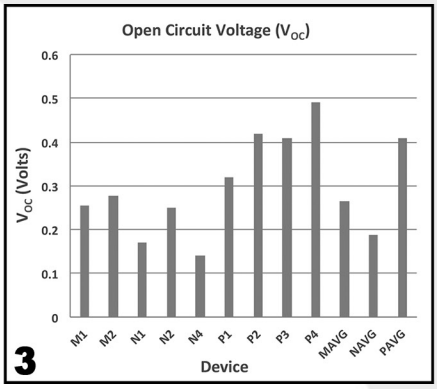

Figure 3: Open-circuit voltages for each device and averages of each device type.

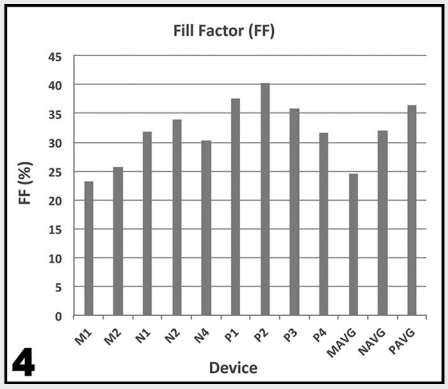

Figure 4: Fill factors for each device and averages of each device type.

(Au) contacts. Heating the wafers removed the tape residue and transferred the WSe_2 flakes onto the Au contacts of the wafers (1c). Four samples were treated with fluoroform after exfoliation and not before. Photolithography techniques were used to create a trench into which a thin film of ITO was sputtered (1d). The optical micrograph of an as-fabricated photovoltaic device made using this process is displayed in (1e) and in Figure 2.

Results and Conclusions:

A semiconductor-parameter analyzer is used for the I-V characterization of all PV devices under the illumination of 532 nm laser light. From the measured I-V characteristics, critical PV performance parameters of all devices, including open-circuit voltages (V_{OC}) (Figure 3) and fill factors (FF) (Figure 4) were determined.

"M devices" refers to MoS_2 cells previously fabricated by Liang's group, while "N devices" refers to n-type-WSe_2/Au structured cells, and "P devices" refers to p-type-WSe_2/Au structured cells. While M cells exhibited a higher average V_{OC} (0.266 V) than N devices (0.187 V), P cells have a higher average V_{OC} (0.410 V) than both M and N devices. Furthermore, P samples exhibit the highest average FF (36.4%), followed by N samples (32.0%) and M samples (24.5%.)

From these data, we can conclude that P devices (i.e., p-type-WSe_2/Au structured cells) exhibit significantly higher V_{OC} and FF parameters in comparison with M and N devices, which are crucial to ultimately obtain unprecedented PCE parameters in the future.

Future Work:

After removing the area of WSe_2 above the gold contact and not below the ITO (i.e., marginal area), power conversion efficiency (PCE), external quantum efficiency (EQE) and short circuit photocurrent density (J_{SC}) data can be obtained for further analysis and comparison. Texturing the surfaces of silicon photovoltaic cells helps contain the light in the P-N junction for a longer time and reduces surface reflections, leading to more generated carriers and a greater photocurrent [2]. This process could significantly enhance the efficiencies of the WSe_2 photovoltaic cells. Also, some LTMDs have not been examined for their efficiencies in the p-n junction of the photovoltaic cell. The same fabrication and testing processes used in this project could be employed for future investigations of newly studied LTMDs.

Acknowledgements:

I would like to thank the NNIN REU Program for selecting me to participate in their research experience. I would also like to acknowledge the National Science Foundation for their funding. Finally, I would like to offer my special thanks to my mentor, Sungjin Wi, and my PI, Xiaogan Liang, for their time and energy spent on guiding me throughout my research.

References:

[1] Wi, S., et al.; "Enhancement of Photovoltaic Response in Multilayer MoS_2 Induced by Plasma Doping"; ACS Nano, 8, 5270-5281 (2014).

[2] Edwards, M., et al.; "Effect of texturing and surface preparation on lifetime and cell performance in heterojunction silicon solar cells"; Solar Energy Materials and Solar Cells, 92, 1373-1377 (2008).

OPTS

Bio-Inspired Surface Treatments and Quasi-Ordered Nanostructures to Control Broadband IR Response

Lesley Chan
Chemical Engineering, University of Southern California

NNIN REU Site: UCSB Nanofabrication Facility, University of California, Santa Barbara, CA
NNIN REU Principal Investigator: Prof. Michael J. Gordon, Chemical Engineering, University of California, Santa Barbara
NNIN REU Mentor: Federico Lora Gonzalez, Chemical Engineering, University of California, Santa Barbara
Contact: lesleywc@usc.edu, mjgordon@engr.ucsb.edu, floragonzalez@umail.ucsb.edu

Abstract:

Moth-eye nanostructures have been fabricated in silicon and germanium using colloidal lithography and reactive ion etching to enhance optical transmission in the near to far infrared wavelength range (λ = 2-50 μm). In previous reports [1, 2], high transmission was achieved using a multi-step etching process to form silicon nanostructures. Here, we demonstrate the fabrication of similar nanostructures using a simplified, single-step vertical etch by systematic modification of etch parameters that include gas flow rates (SF_6/C_4F_8/Ar), RF power, and etch time. Using this method, fabrication of moth eye nanostructures on germanium (Ge) was also achieved. Nanostructures were optically characterized via Fourier transform infrared spectroscopy (FTIR). High transmission was observed for Si and Ge, for both single-sided (Si: ~94% of theoretical limit, Ge: ~97% of theoretical limit) and double-sided (Si: ~88% absolute transmission, Ge: ~92% absolute transmission) moth-eye samples.

Introduction:

Recent developments in nanotechnology have shown a need for enhanced anti-reflective coatings (ARCs) for infrared (IR) devices such as thermophotovoltaics, optoelectronics, and IR detectors. These mentioned devices are typically made from high refractive index materials, such as silicon (Si), resulting in large reflective losses. Conventional ARCs are composed of vacuum-deposited thin film dielectric materials that are known to have low acceptance angles and can only enhance transmission at specific designed wavelengths. Multi-layer ARCs can overcome some of these issues, but the deposition is time consuming, expensive, and substrate dependent. Therefore, we present "bio-inspired" moth-eye (ME) nanostructures for anti-reflection, depicted in Figure 1, that operate by the introduction of a refractive index gradient, which not only provides superior broadband anti-reflection, but fabrication is both quick and simple.

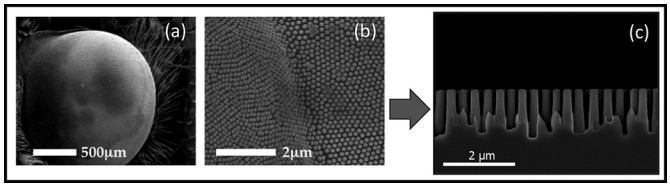

Figure 1: (a) SEM images of moth's eye showing hexagonally packed nanostructures [2]. (b) SEM image of moth-eye nanostructures fabricated on Si.

Typically, ME nanostructures have been used for anti-reflection in the visible range, but our work focuses on IR wavelength ranges. ME nanostructures are also scalable and substrate-independent, which means they can be theoretically implemented for any wavelength range and any material. Furthermore, using a simplified single-step vertical etch method, as opposed to a multi-step Bosch etch plus isotropic ICP-RIE as reported previously [1, 2], we were able to make high-performance and robust ME nanostructures.

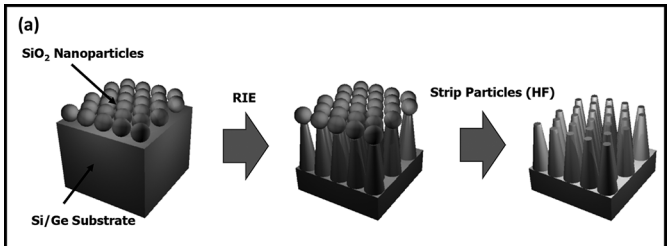

(b)

Etch Parameter	Si	Ge
Nanoparticle Size	380 nm	540 nm
ICP Power	825 W	825 W
Bias Power	15 W	20 W
SF_6/C_4F_8/Ar	26/54/20 sccm	24/56/20 sccm
Pressure	19 mTorr	19 mTorr

Figure 2: (a) Process scheme to create moth eye anti-reflectors: fabrication of nanostructures started with SiO_2 mask deposition using Langmuir-Blodgettry, followed by reactive ion etching, and stripping of SiO_2 using HF. The process is repeated on the backside of the wafer to form double-sided nanostructures. (b) Etch parameters for reactive ion etching for both Si and Ge.

Experimental Procedure:

Fabrication of ME nanostructures was done using a simple, two-step colloidal lithography method as shown in Figure 2.

OPTS

The silica nanoparticle mask was deposited on Si (University wafer, 225 μm thick, > 4000 Ohm-cm) and Ge (MTI Corp., 500 μm thick, > 50 Ohm-cm) wafers using a Langmuir-Blodgett dip coating process [1-3]. The nanoparticle sizes used were 380 and 540 nm for Si and Ge, respectively. Afterward, masked Si and Ge samples were plasma-etched (Plasma-Therm 770 SLR-RIE) using a single-step vertical etch with varying conditions for gas flow rates (SF_6/C_4F_8/Ar), bias power, and etch time as summarized in Figure 2.

After plasma etching, the silicon dioxide (SiO_2) nanoparticles were subsequently stripped using hydrofluoric acid (10%). The colloidal lithography process was repeated on the backside of the substrate to fabricate double-sided ME substrates. The ME nanostructures were characterized using scanning electron microscopy (SEM) for morphology and FTIR for transmission.

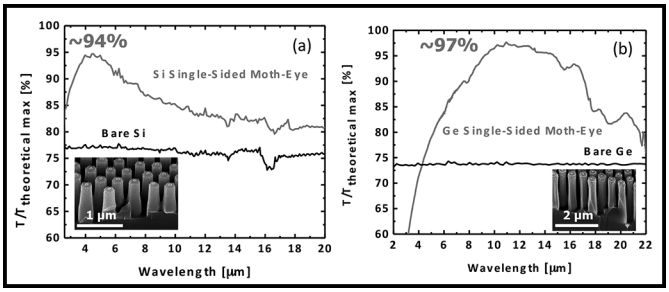

Figure 3: Normalized transmission with respect to theoretical maximum (Si: T_{max} ~ 70%, Ge: T_{max} ~ 64%) for single-sided ME nanostructures on Si and Ge and corresponding cross-sectional SEMs.

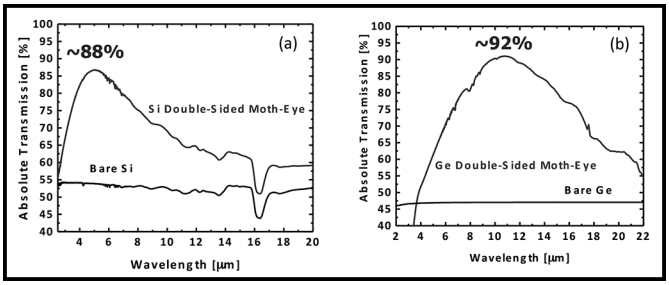

Figure 4: Absolute transmission for double-sided ME nanostructures on Si and Ge.

Results and Conclusions:

The theoretical maximum transmission was calculated to be ~ 70% for single-sided ME in Si and ~ 64% for single-sided ME in Ge. Direct transmission for single-sided Si and Ge nanostructured substrates had a peak transmission of 94% and 97% of the theoretical maximum, respectively, as shown in Figure 3. By implementing nanostructures on both sides of the substrate, the theoretical maximum increases to 100% in both materials.

Direct transmission for double-sided Si and Ge nanostructured substrates had a peak of 88% and 92% absolute transmission, respectively, as shown in Figure 4. Furthermore, by changing nanoparticle size, we were able to adjust the pitch, resulting in peak transmission wavelength shifting. For the 380 nm nanoparticle masks on Si, the resulting peak position for double-sided occurred at λ = 5.5 μm, while for 540 nm nanoparticle masks on Ge, the peak position for double-sided occurred at λ = 10.8 μm. This demonstrates the tunability of the IR response by simply modifying mask size.

Future Work:

In conclusion, using Langmuir-Blodgettry and a single-step vertical etch in different materials platforms to produce ME nanostructures, we were able to achieve high optical transmission in the IR. High increases in transmission were observed for both single-sided (Si: ~ 94% of theoretical limit, Ge: ~ 97% of theoretical limit) and double-sided (Si: ~ 88% absolute transmission, Ge: ~ 92% absolute transmission) nanostructures.

With further optimization of mask deposition and etch parameters, we can achieve even better anti-reflective properties, yielding higher IR transmission and also demonstrate the ability to produce ME nanostructures in additional materials.

Acknowledgements:

I would like to thank Professor Michael Gordon, my mentor Federico Lora Gonzalez, and Professor Daniel Morse for their help and guidance this summer, as well as Alex Berry for his help in nanoparticle synthesis and mask deposition. I would also like to thank the UCSB cleanroom staff for help with the plasma etching. This work was supported by the National Nanotechnology Infrastructure Network Research Experience for Undergraduates Program, the National Science Foundation, and the Institute for Collaborative Biotechnologies.

References:

[1] Federico Lora Gonzalez, Daniel E. Morse, Michael J. Gordon, Opt. Lett. 39, 13-16 (2014).

[2] Federico Lora Gonzalez, Michael J. Gordon, Opt. Express 22, 12808-12816 (2014).

[3] Federico Lora Gonzalez, Lesley Chan, Alex Berry, and Michael J. Gordon. JVST B (Submitted 2014).

OPTS

Study of Cerium Doped Terbium Iron Garnet Thin Films for Magneto-Optical Applications

Emiliana Cofell
Physics, Scripps College

NNIN REU Site: Minnesota Nano Center, University of Minnesota-Twin Cities, Minneapolis, MN
NNIN REU Principal Investigator: Prof. Bethanie Stadler, Electrical and Computer Engineering, Chemical Engineering and Materials Science, University of Minnesota-Twin Cities
NNIN REU Mentor: Prabesh Dulal, Chemical Engineering and Material Science, University of Minnesota-Twin Cities
Contact: ercofell@gmail.com, stadler@umn.edu, dulal002@umn.edu

Abstract:

Thin films of magneto-optical materials are useful in optical isolators, which are devices used in photonic circuits as "optical diodes" to prevent reflected light from damaging the laser source. This is achieved by an effect called Faraday rotation, which is a rotation of the polarization of light when passing through a magneto-optic material. The material studied in this project was cerium doped terbium iron garnet (Ce:TIG/$Ce_xTb_{3-x}Fe_5O_{12}$). The thin films were deposited on silicon and fused quartz substrates using reactive sputtering in an oxygen environment. The iron and terbium targets were sputtered at a constant power while the cerium power was varied to change the cerium concentration. The samples were annealed at 700°C, 800°C, and 900°C using rapid thermal annealing (RTA). The characterization of the samples included measuring the Faraday rotation using an optics bench setup with a 1545 nm laser. A correlation between increasing cerium content and the Faraday rotation was observed. Future work will include developing optical isolators with Ce:TIG as the magneto-optical material on a silicon platform for use in photonic circuits.

Introduction:

Optical isolators are important for use in waveguides for integrated photonic circuits; these devices prevent reflected light from damaging the laser source. Magneto-optical materials are useful for the development of optical isolators due to their ability to rotate the polarization of light through the Faraday Effect [1]. This effect, $\beta = vBd$, relates the angle of rotation of the polarization (β) to the Verdet constant (v) of the material, applied magnetic field (B), and thickness of the material (d) [2]. In this project, thin films of the magneto-optical material cerium-doped terbium iron garnet (Ce:TIG) were developed and the amount of cerium deposited in the thin films was varied in order to measure the magneto-optical properties and optimize the Faraday rotation.

Experimental Procedure:

The samples were deposited using an oxygen reactive sputtering process on silicon and fused quartz substrates. We used three targets in the sputtering chamber: iron, terbium, and cerium. The sputtering power for iron was fixed at 220 W, terbium at 110 W, and the cerium power was varied from 0-100 W in 10 W intervals. We then annealed three samples from each batch, one each at 700°, 800° and 900°C.

We were able to achieve the garnet phase from 0-50 W cerium when these samples were annealed at either 800° or 900°C. Annealing at 900°C for two minutes formed the best garnet out of all our samples. We were also able to achieve the garnet phase from 30-50 W cerium on GGG substrates.

After checking for crystallization using x-ray diffraction (XRD), we further characterized the samples using a scanning electron microscope (SEM), vibrating sample magnetometer (VSM), energy-dispersive x-ray spectroscopy (EDS), and an optics bench setup with a 1545 nm laser to measure the Faraday rotation coefficient of the samples.

Results and Conclusions:

In observing the samples with the SEM, cracking of various sizes was noted on most samples due to a mismatch in the thermal expansion coefficients between the substrate and thin films (see Figure 1); however, this can be eradicated in actual waveguide development by patterning the samples before deposition [1].

Some challenges were encountered when measuring the atomic percentage of cerium contained in the samples with EDS, due to non-uniform composition of the samples from the sputtering process and initial technical difficulties with the EDS. The results were somewhat surprising, as increased cerium sputtering power did not always directly relate to increased atomic percent of cerium, as is shown in Figure 2. This was most likely due to variability in the bias voltage

OPTS

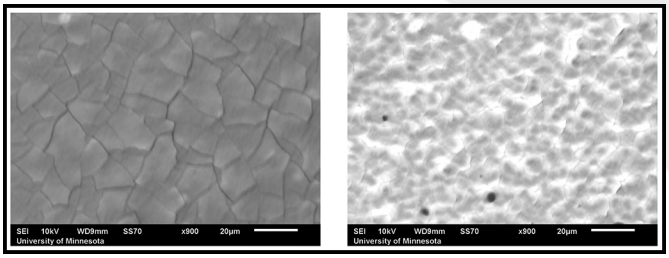

Figure 1: SEM images showing various irregularities in samples. The left image is from a sample with 30 W cerium; the right image is from a sample with 60 W cerium, which did not form garnet. Both samples are on silicon substrates.

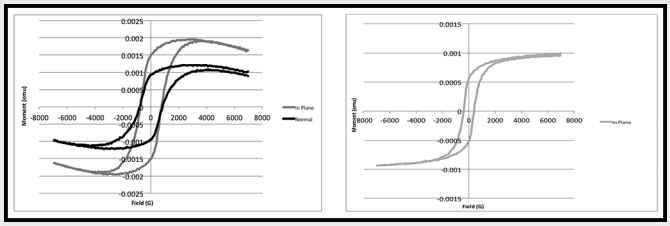

Figure 3: VSM measurements. [Left] Initial VSM measurements for the sample with 20 W cerium. [Right] VSM measurements after subtracting silicon contributions (used in-plane loop only).

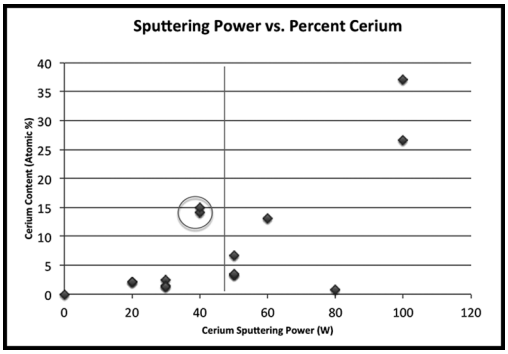

Figure 2: EDS results were slightly inconsistent — the dark grey vertical line represents the cutoff of samples that were able to form garnet. Circled data points represent the garnet sample with the highest atomic percent of cerium.

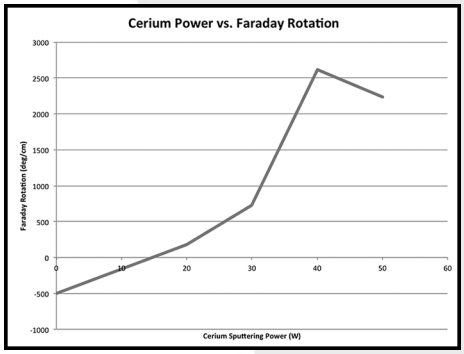

Figure 4: Faraday rotation measurement results.

during the sputtering process, and further sample creation to gather additional data will be necessary in the future.

Measurements with the VSM were also initially challenging, as many of the hysteresis loops were slanted or did not close at one end, which did not agree with previous results from similar samples. We hypothesized that this could be explained by contributions from the silicon substrates, and were able to correct for this by subtracting readings from blank silicon for some of the measurements (see Figure 3).

The Faraday rotation measurements were promising for the samples; large negative Faraday rotations of -2240° cm^{-1} and -2620° cm^{-1} were observed for the two garnet samples with the largest atomic percentage of cerium. In general, a positive correlation between cerium content and Faraday rotation was observed, shown in Figure 4. However, due to irregularities in the sputtering process future characterization will be required to confirm this.

Future Work:

More sample fabrication and characterization will be necessary to determine the optimal recipe for Ce:TIG that produces the greatest Faraday rotation. After this has been determined, waveguides can be fabricated and tested for eventual use in photonic circuits.

Acknowledgements:

I would like to thank Professor Beth Stadler for the opportunity to work in her lab on this project, as well as Prabesh Dulal for all his guidance and advice. I would also like to acknowledge the University of Minnesota CharFac where part of this work was carried out, which is partially funded by MRSEC. I would like to thank the NNIN REU Program and the NSF for funding this project.

References:

[1] Dulal, P., Block, A.D., Haldren, H.A., Hutchings, D.C., Sung, S.Y., and Stadler, B.J.H. "TIG without Seedlayers on Semiconductor Substrates." Applied Physics Letters (to be published in 2014).

[2] Dulal, P. "Development of Novel Iron Garnet Thin Films for Magneto-optical Applications." A proposal submitted to the ChemE and MSE faculty and the Graduate School of the University of Minnesota by P. Dulal in partial fulfillment of the requirement of the candidacy for the degree of Doctor of Philosophy.

OPTS

Particle Sorting on Microfluidic Chips using Optical Forces

Brandon Foley
Chemical Engineering, University of Wisconsin – Madison

NNIN REU Site: Center for Nanoscale Systems, Harvard University, Cambridge, MA
NNIN REU Principal Investigator: Federico Capasso, Physics, Harvard University
NNIN REU Mentors: Lulu Liu and Alexander Woolf, Physics, Harvard University
Contact: brfoley@wisc.edu, capasso@seas.harvard.edu, lululiu@fas.harvard.edu, awoolf@fas.harvard.edu

Introduction:

Sorting particles using light can provide another means for particles separation. On-chip particle sorting has been used to sort particles based on size or using dielectrophoretic forces [1]. Optical forces can be used to sort particles that have similar chemical, physical, and electromagnetic properties, but different optical properties. It is especially difficult to separate particles that are enantiomers of each other, which have identical chemical and physical properties and differ only in their interactions with light. The scattering of circularly polarized light is dependent on the handedness of the chiral particle and of the circularly polarized light [2]. This difference in scattering will be used to push particles in different directions on a microfluidic chip. The microfluidic chip is a channel ending in a fork. The particles flow down the channel and are pushed either left or right, depending on the particle's handedness, causing the particles to travel the channel in the direction it was pushed. The goal of this study is to fabricate a flow chamber capable of sorting particles using optical forces.

Methods:

SU-8 Master Wafer Synthesis. The SU-8 master wafer was made using SU-8-3025 at a thickness of 20 μm using negative photoresist methods as outlined by MicroChem [3].

Flow Chamber Synthesis. The standard 10:1 monomer:cross-linking agent ratio for polydimethylsiloxane (PDMS) was mixed and degassed before pouring over the silicon master chip in a Petri® dish to a thickness of approximately 1 cm. The Petri® dish was then placed in an oven at 65°C for three hours. The PDMS was removed from the silicon wafer and plasma oxidized to adhere it to a glass slide. A 1.20 mm hole was punched in channel and a 1/16-inch O.D. tubing attached to flow the bead suspension into the microfluidic flow chamber, as shown in Figure 1.

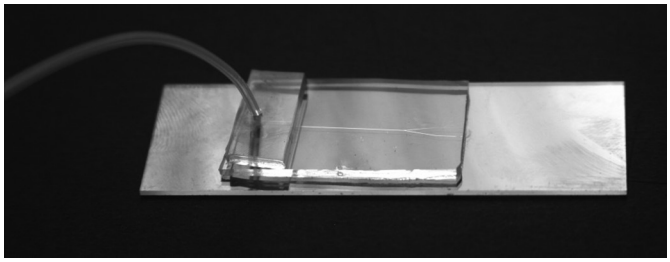

Figure 1: A PDMS flow chamber prototype for particle sorting using optical forces.

Controlling Flow Rate. The velocity of the beads needed to be slow so there would be enough interaction time with the laser for sufficient displacement to occur. The desired flow rate was 0.02 μL/h. Gravity was used as the driving force for the flow, and was controlled by installing two needle valves to increase or reduce the friction to adjust the flow rate through the microfluidic flow chamber.

Experiment. Glass beads with a diameter of 5 μm were flowed through the flow chamber at a rate of 10-30 μm/s. A 660 nm laser was shown on the beads to the right at a power of 3.2×10^{-4} mW/μm^2. The distribution of the beads at the fork were counted in the presence of the laser and compared to the distribution of the beads without the laser.

Results and Discussion:

The flow chamber successfully sorted beads using optical forces, as shown by the results in Table 1. Using Flow Chamber A, without the presence of radiation pressure, 50.8% ± 7.0% of the beads were entering the left channel at the fork. When 3.2×10^{-4} mW/μm^2 of radiation pressure was exerted on the beads towards the right, the fraction of beads travelling down

OPTS

the left channel decreased to 35.7% ± 6.3%. This verifies that optical forces are capable of potentially sorting particles.

Consistency was another important measure of the flow chambers. Flow chambers with the same design should behave similarly and the same flow chambers should have consistent behavior over time. As shown in Table 1, this was not the case for these flow chambers.

Chamber	Conditions	Left	Right	Total	Fraction Left	Error	Lower Bound	Upper Bound
A	Null	100	97	197	0.508	0.070	0.438	0.577
A	Laser Right, 3.2 x 10-4 mW/μm^2	79	142	221	0.357	0.063	0.294	0.421
B	Null	162	40	202	0.802	0.055	0.747	0.857
B	Laser Right, 3.2 x 10-4 mW/μm^2	164	75	239	0.686	0.059	0.627	0.745
B	Laser Left, 3.2 x 10-4 mW/μm^2	138	60	198	0.697	0.064	0.633	0.761
B	Null, retrial	56	60	116	0.483	0.091	0.392	0.574

Table 1, above: Results from preliminary experiments evaluating ability of optical forces to change distribution of beads.

Flow Chamber B had 80.2% ± 5.5% without the presence of radiation pressure, which is significantly higher Flow Chamber A. The behavior of Flow Chamber B also changed during experiments. The fraction of beads that travelled down the left channel at the fork after the experiments was 48.3% ± 9.1%. This difference suggests that morphological changes occurred. This could have been caused by dust clogging or unclogging from the channels or from beads sticking to the PDMS walls, causing a change in the flow. An example of clogging is shown in Figure 2.

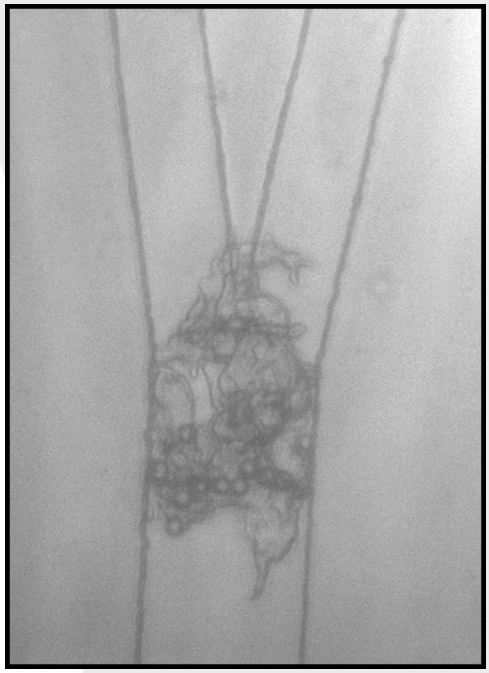

Figure 2, right: Dust clogging in the flow chamber at the fork.

Future Work:

To resolve issues involving dust clogging of channels, a filter will be added to the flow chamber. The filter consists of diamond-shaped pillars with decreasing gap sizes designed to block any pieces of dust that may clog the channel, while letting the beads pass through freely. Currently, there is a slight attraction between the beads and the PDMS walls. With a filter consisting of PDMS pillars, bead sticking may become a more important issue. To prevent bead sticking, the PDMS will be coated with negatively charged polymer. The glass beads naturally retain a negative charge, or polystyrene beads with carboxylic acid groups on the surface can be used, giving a negative charge to the polystyrene beads. The repulsion between the like-charges of the PDMS walls and the beads will prevent the beads from sticking to the filter or anywhere along the channels.

Acknowledgements:

I would like to thank Professor Federico Capasso for allowing me to join his group this summer, my mentors Lulu Liu and Alex Woolf for their support and guidance, the rest of the Capasso group, and the Harvard site coordinators Kathryn Hollar and Sara Wenzel for helping set up the program. I would also like to thank the National Nanotechnology Infrastructure Network Research Experience for Undergraduates Program and the National Science Foundation for their financial support.

References:

[1] K. Ahn, et al., Dielectrophoretic manipulation of drops for high-speed microfluidic sorting devices. Appl. Phys. Lett. 88, 024104 (2006). http://dx.doi.org.ezproxy.library.wisc.edu/10.1063/1.2164911.

[2] Singham, Shermila Brito, Form and intrinsic optical activity in light scattering by chiral particles. J. Chem. Phys. 87, 1873 (1987). http://dx.doi.org.ezproxy.library.wisc.edu/10.1063/1.453202.

[3] MicroChem. SU-8 3000 Permanent Epoxy Negative Photoresist http://www.microchem.com/pdf/SU-8%203000%20Data%20Sheet.pdf.

Opto-Electronic Characterization of Narrow Band Gap Semiconductors at Cryogenic Temperatures

Chanud Yasanayake
Physics, Pomona College

NNIN REU Site: UCSB Nanofabrication Facility, University of California, Santa Barbara, CA
NNIN REU Principal Investigator: Christopher Palmstrøm, Department of Electrical and Computer Engineering, University of California, Santa Barbara
NNIN REU Mentor: Mihir Pendharkar, Electrical and Computer Engineering, University of California, Santa Barbara
Contact: chanudn@gmail.com, cpalmstrom@ece.ucsb.edu, mihir@ece.ucsb.edu

Introduction:

Semiconductors are fundamental to modern technology, with uses ranging from scientific research to commercial applications in computing and telecommunications. There is a great deal of interest in studying these materials, both to improve their use in current technologies and to discover potential future applications in novel devices.

In this work, we focused on a characterization apparatus used for studying semiconductors (see Figure 1). This apparatus optically probed a semiconductor sample with a 532 nm Nd:YAG solid-state laser and used a monochromator and detector to generate the sample's photoluminescence (PL) spectrum. This spectrum can then be used to determine the material's band gap, an important physical property. In addition, the band gap's temperature dependence can be investigated by placing the sample in a 10 K cryostat.

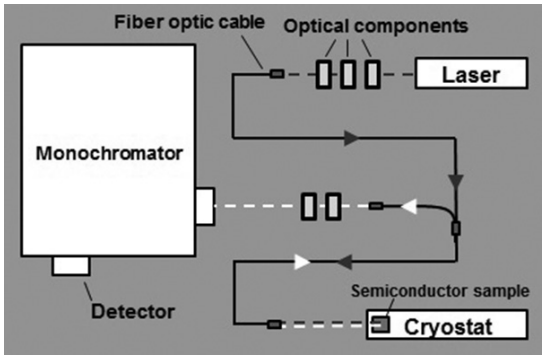

Figure 1: Characterization apparatus diagram. Laser light shown in gray, photoluminescence in white.

The characterization apparatus was formerly only capable of optically probing semiconductors that photoluminesce visible to near infrared light. Major modifications were made to this apparatus to add to its functionality so that it could: (1) employ electrical measurements in addition to optical probing, and (2) detect narrow band gap semiconductors, which photoluminesce with mid to far infrared light. These modifications entailed both redesigning existing parts of the apparatus using the CAD software SolidWorks and incorporating new components into the setup.

Modifications:

The limitations of the apparatus were narrowed down to three major areas: the optical components, the cryostat, and the monochromator. Modifications were made to these areas to overcome their respective limitations.

The optical components were not positioned optimally, resulting in a low signal to noise ratio. This was corrected by repositioning each component individually until the signal was maximized. There was also an issue with noise from the laser; although the laser nominally lases at 532 nm, it is a frequency doubled laser that has significant lasing at 1064 nm as well. It also has significant emissions at several wavelengths near 532 nm. These two issues were resolved with the addition of two new filters, one to block light at 1064 nm and one to block light near 532 nm while still transmitting 532 nm light.

The cryostat (see Figure 2) had several distinct limitations to consider. For one, it took up to two hours to cool down from room temperature

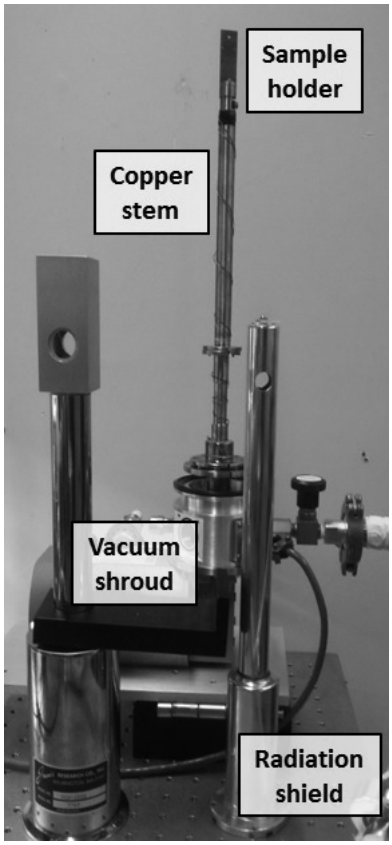

Figure 2: The former cryostat, disassembled. Labeled components were modified.

OPTS

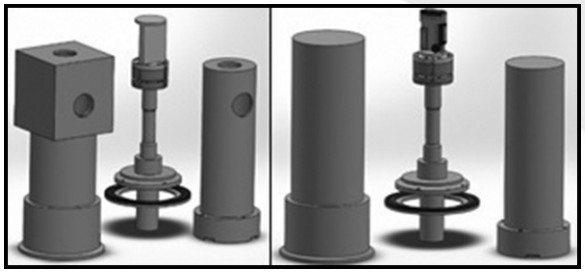

Figure 3: SolidWorks models of both versions of the new cryostat components, optical (left) and electrical (right).

to 10 K. The cryostat vacuum shroud windows absorbed mid to far infrared light, which prevented detection of the photoluminescence of narrow band gap semiconductors. The sample holder did not allow for wiring of the sample, a necessity for making electrical measurements. The modifications needed to overcome these problems yielded two sets of new cryostat components, an optical version and an electrical version (see Figure 3).

Both versions have a much shorter copper stem. This reduces cooling time since the sample holder is cooled by contact with this stem, which is in turn cooled by contact with the cryostat. The optical version has a vacuum shroud and radiation shield that accommodate new CaF_2 windows, which transmit visible to far infrared light (0.2-8 μm) and can therefore be used for narrow band gap semiconductor PL studies (i.e., InAs, InSb). The electrical version has a sample holder that supports the addition of 16 pin DIP sockets, which can be wired for electrical measurements. The electrical version also has a windowless vacuum shroud and radiation shield, which can be used when studying samples whose electrical properties are affected by ambient light.

There were four detectors that could be used with the monochromator. Two of them, an InGaAs detector and a photomultiplier tube, could be mounted onto the monochromator but could only detect light with wavelengths up to 1.8 μm, below the mid to far infrared regime. The other two detectors, InAs and HgCdTe, could detect mid to far infrared (up to 3.8 μm and up to 12 μm, respectively), but were not designed to be mounted onto the monochromator. Therefore, mounting plates were made for properly positioning the InAs and HgCdTe detectors on the monochromator where light would be focused on the detectors.

Testing:

Preliminary tests on the completed modifications suggest they are fully functional. In particular, photoluminescence spectra

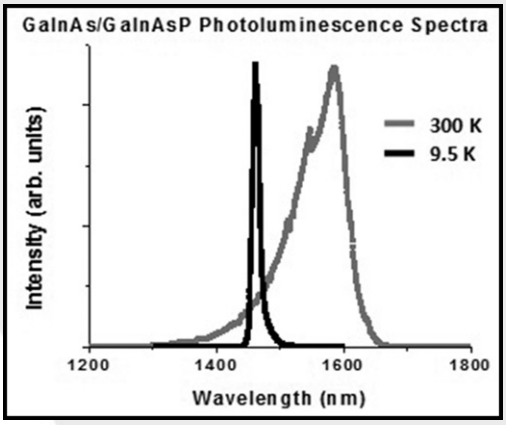

Figure 4: Photoluminescence spectra for GaInAs/GaInAsP sample at 300 K (room temperature) and at 9.5 K.

of a GaInAs/GaInAsP sample (see Figure 4) exhibited well-defined peaks both at room temperature and at 9.5 K in the cryostat, indicating that the optical alignment and new filters were yielding a satisfactory signal to noise ratio for making measurements. The signal was also clear enough to observe the peak being narrower and shifted to a smaller wavelength for the 9.5 K spectrum, an expected occurrence that shows the temperature dependence of band gap.

Future Work:

Most of the modifications have been completed and have undergone initial testing with promising results. The electrical sample holder still has to be wired for electrical measurements and the fiber optic cable will need to be replaced as it only transmits up to a wavelength of 2.5 μm. This limits the operating range of the upgraded setup, as all the modified parts function at wavelengths up to 8 μm. Further testing is required when all parts are complete and the functionality of the apparatus can be assessed as a whole.

Acknowledgements:

I would like to thank my mentor, Mihir Pendharkar, for his extensive guidance throughout this project, as well as my principal investigator Professor Chris Palmstrøm and the rest of the Palmstrøm group. The UCSB Physics Machine Shop staff were also incredibly helpful, machining the parts we designed and providing design advice. This work was supported and funded by the National Nanotechnology Infrastructure Network Research Experience for Undergraduates (NNIN REU) Program; the University of California, Santa Barbara; and the National Science Foundation.